Invest New Drugs (2015) 33:541–554
DOI 10.1007/s10637-015-0215-9

PRECLINICAL STUDIES

Combretastatin A-4 derived imidazoles show cytotoxic, antivascular, and antimetastatic effects based on cytoskeletal reorganisation

Katharina Mahal · Bernhard Biersack · Henrike Caysa · Rainer Schobert · Thomas Mueller

Received: 5 January 2015 / Accepted: 1 February 2015 / Published online: 14 February 2015

Summary *Introduction* Combretastatin A-4 (CA-4) is a natural *cis*-stilbene which interferes with the cellular tubulin dynamics and which selectively destroys tumour blood vessels. Its pharmacological shortcomings such as insufficient chemical stability, water solubility, and cytotoxicity can be remedied by employing its imidazole derivatives. *Methods* We studied 11 halogenated imidazole derivatives of CA-4 for their effects on the microtubule and actin cytoskeletons of cancer and endothelial cells and on the propensity of these cells to migrate across tissue barriers or to form blood vessel-like tubular structures. *Results* A series of *N*-methyl-4-aryl-5-(4-ethoxyphenyl)-imidazoles proved far more efficacious than the lead CA-4 in growth inhibition assays against CA-4-resistant HT-29 colon carcinoma cells and generally more selective for cancer over nonmalignant cells. Et-brimamin (**6**), the most active compound, inhibited the growth of various cancer cell lines with IC_{50} (72 h) values in the low nanomolar range. Active imidazoles such as **6** reduced the motility and invasiveness of cancer cells by initiating the formation of actin stress fibres and focal adhesions as a response to the extensive microtubule disruption. The antimetastatic properties were ascertained in 3D-transwell migration assays which simulated the transgression of highly invasive melanoma cells through the extracellular matrix of solid tumours and through the endothelium of blood vessels. The studied imidazoles exhibited vascular-disrupting effects also against tumour xenografts that are refractory to CA-4. They were also less toxic and better tolerated by mice. *Conclusions* We deem the new imidazoles promising drug candidates for combination regimens with antiangiogenic VEGFR inhibitors.

Keywords Combretastatin A-4 · Imidazoles · Vascular-disrupting agents (VDA) · Antimetastatic activity · Transwell invasion assay · Trans-endothelium migration assay · CAM assay

Introduction

The *cis*-stilbene combretastatin A-4 (CA-4; Fig. 1a) which was first isolated from the South-African bushwillow *Combretum caffrum* shows a remarkable antivascular activity [1, 2]. CA-4 and its clinically investigated phosphate prodrug fosbretabulin (CA-4P) are vascular-disrupting agents (VDA) which selectively target the blood vessels of solid tumours [3–5]. CA-4 binds primarily to the colchicine binding site of beta-tubulin and impedes the polymerisation of heterodimeric tubulin subunits to give microtubules [2, 6]. Its antiproliferative effect is based mainly on this disruption of the highly organised microtubule cytoskeleton. Cells affected in this way are hindered to develop mitotic spindles leading to mitotic arrest and eventually to apoptosis [4, 7–9]. In contrast, the disruption of blood vessels by CA-4 or CA-4P is an immediate effect originating from a rapid change of the morphology of individual endothelial cells and a perturbation of the integrity of endothelial cell monolayers. Investigations into the signalling pathways involved in the cellular response to inhibitors of microtubule formation showed the small GTPase Rho, Rho-associated kinase (Rho-kinase) and various mitogen-

Electronic supplementary material The online version of this article (doi:10.1007/s10637-015-0215-9) contains supplementary material, which is available to authorized users.

K. Mahal · B. Biersack · R. Schobert (✉)
Organic Chemistry Laboratory, University Bayreuth, Universitaetsstrasse 30, 95440 Bayreuth, Germany
e-mail: rainer.schobert@uni-bayreuth.de

H. Caysa · T. Mueller
Department of Internal Medicine IV, Oncology/Hematology, Martin-Luther-University Halle-Wittenberg, 06120 Halle-Saale, Germany

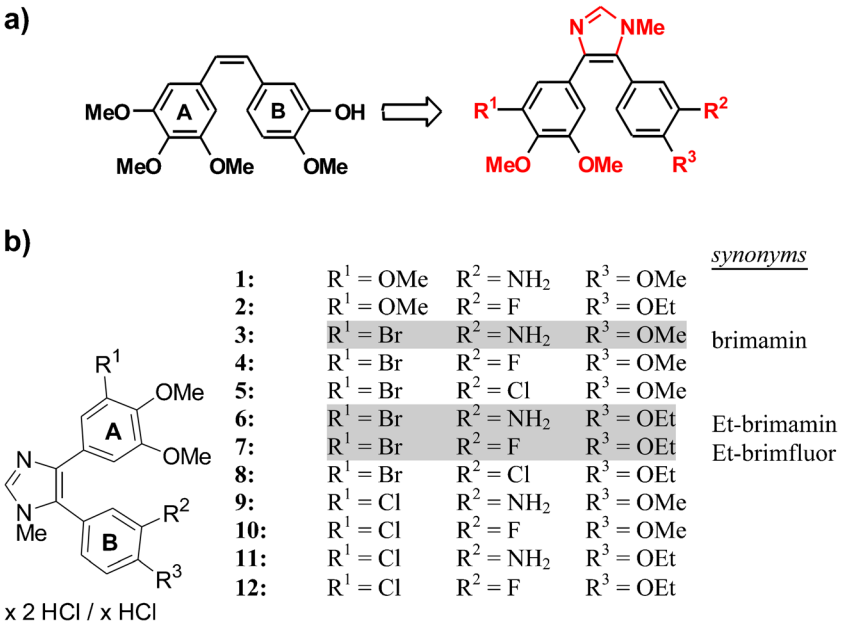

Fig. 1 Structures of combretastatin A-4 (CA-4) and imidazole analogues. **a**) Structure of CA-4 with A- and B-ring denotation and of imidazole analogues with various substitution sites. **b**) Structures of N-methyl-4-(4,5-dimethoxyphenyl)-5-phenyl-imidazolium hydrochlorides **1**–**12** with variation in residues R^1, R^2, and R^3 as specified. Important compounds highlighted and assigned short names

activated protein kinases (MAPKs) to play an essential role. Typical effects of CA-4 are the assembly of actin stress fibres, an increase in cell contractility, a loss of cell-cell contacts and the induction of apoptosis [10–12]. They are responsible for the disruption of the tight cellular organisation of the endothelium, the increase in endothelial permeability, and the leaking or disruption of tumour blood vessels. The consequences visible in solid tumours are haemorrhages and necrosis [3, 4, 13]. Unfortunately, CA-4 is not suitable for clinical application because of its metabolic conversion to the inactive *trans*-isomer and its insufficient solubilty and cytotoxicity [2, 5]. Although the irregular vasculature of solid tumours is a promising drug target the number of clinically tested antivascular drugs is still rather small. Examples are the CA-4 serinyl prodrug AVE8062 [14, 15] and the CA-1 diphosphate prodrug OXi4503 [16]. More recently, combretastatin A derivatives with imidazole, oxazole or other heterocycles bridging the alkene bond were developed that retain the vascular-disrupting effect while showing an enhanced chemical stability and cytotoxicity [17–20]. Lately, we developed a series of *N*-methylimidazole-brigded CA-4 derivatives bearing *meta*-halogen substituents at the A- or B-ring (Fig. 1b) and optimised their antitumoural and antivascular properties both in vitro and in vivo [18, 19].

The current paper presents a new series of five halogenated imidazole analogues of CA-4 (**6**–**8**,**11**,**12**) which share a *meta*-halogen substituted A-ring and a B-ring with *meta*-halogen/NH_2 and *para*-OEt substitution. With both series of imidazoles in hand we could now study the influence of various substituent constellations on their cytotoxicity, vascular-disrupting activity in vitro and in vivo, their cancer selectivity, and the underlying cellular mechanisms, also in comparison to the lead compound CA-4. Particularly insightful was a comparison of imidazole couples that differ only in the *para*-substituent on the B-ring, being either the original methoxy group of CA-4 or an ethoxy group, i.e., **3**/**6**, **4**/**7**, **5**/**8**, **9**/**11**, and **10**/**12**.

Materials and methods

Imidazoles, stock solutions and dilution series

CA-4 was purchased from Sigma Aldrich. The known imidazoles **1**–**4** were prepared as published [17–19], the new derivatives **5**–**8**,**11**,**12** were synthesised analogously (cf. Electronic supplementary material). Stock solutions were prepared by dissolving CA-4 and the purified imidazolium hydrochlorides **2**–**12** in DMSO to a final concentration of 10 mM. All dilution series were prepared in 1 × PBS or ddH_2O.

Cell lines and culture conditions

The human carcinoma cell lines HT-29 (colon), HCT-116 (colon), and MCF-7 (breast) were purchased from The German Collection of Microorganisms and Cell Culture (DSMZ, Braunschweig). MCF-7 cells were rendered multidrug-resistant, indicated as MCF-7/Topo, by repeated application of topotecan. Primary human umbilical vein endothelial cells (HUVEC) were obtained from DSMZ and the HUVEC-derived endothelial hybrid cell line Ea.hy926 from The American Type Culture Collection (ATCC no. CRL-2922). The human melanoma cell line 518A2 was a gift from the Department of Radiotherapy and Radiobiology, University Hospital Vienna. It is not available from cell banks, yet easily identified by its large size and its flat, spread-out morphology. Cells of

cell lines 518A2, HT-29, HCT-116, MCF-7/Topo, and Ea.hy926 were grown in DMEM or RPMI (HT-29) medium, supplemented with 10 % fetal bovine serum (FBS), 1 % Antibiotic-Antimycotic solution (both from Gibco) and 250 μg/mL gentamycin (SERVA). Experiments with HUVEC were conducted at the Helmholtz Centre for Infection Research (Braunschweig, Germany). HUVEC were cultured in EGM-2 medium (Lonza). Primary chicken heart fibroblasts (CHF) were explanted from 10 day-old chicken embryos and separated from other cell types for several weeks. The established cell line based on single fibroblasts was finally grown in DMEM (10 % FBS, 1 % Anti-Anti, 250 μg/mL gentamycin) and used before the 20th passage. All cells were incubated at 37 °C, 5 % CO_2, 95 % humidified atmosphere. Only mycoplasm-free cell cultures were used.

Cell cycle analyses

CA-4-sensitive 518A2 melanoma cells (2×10^5 cells/well) grown on 6-well cell culture plates were treated with DMSO (control), CA-4 (5 nM) or the imidazole derivatives **3** (25 nM) and **6** (10 nM). HT-29 colon carcinoma cells (2×10^5 cells/well) were treated with vehicle or compounds **3** or **6** (100 nM). Since HT-29 are resistant to CA-4 [21, 22], a higher concentration of CA-4 (10 μM) was used to observe comparable effects on the cell cycle. After incubation for 24 h, cells were harvested by trypsination, fixed (ice-cold 70 % EtOH, 1 h, 4 °C), and incubated with propidium iodide (PI, Carl Roth) staining solution (50 μg/mL PI, 0.1 % sodium citrate, 50 μg/mL RNase A in PBS) for 30 min at 37 °C. The fluorescence intensity of 10,000 single cells at an emission wavelength of 620 nm (exCitation with a 488 nm laser source) was recorded with a Beckman Coulter Cytomics FC500 flow cytometer and analysed for the distribution of single cells (%) to G1, S and G2-M phase of the cell cycle as well as for the content of sub-G1 events (apoptotic cells) by using the CXP software (Beckman Coulter).

Determination of the mitotic index

518A2 or HT-29 cells (1×10^4 cells/well) grown on glass coverslips were allowed to adhere for 24 h and then exposed to CA-4 (518A2: 5 nM CA-4, HT-29: 5 μM CA-4) or to imidazoles **3** and **6** for 6 h. After fixation with 4 % formaldehyde in PBS for 20 min, coverslips were washed twice with PBS and mounted in Mowiol 4-88-based mounting medium containing 1 μg/mL DAPI (4′,6-diamidino-2-phenylindole) overnight at 4 °C. Pictures of DAPI-stained nuclei in random fields of the slides were recorded with a ZEISS Axiovert 135 fluorescence microscope (AxioCam MRc5, 400-fold magnification). For each concentration a minimum of 800 cells from at least four pictures were counted (AxioVision software) and the percentage of mitotic cells was calculated from the ratio of mitotic cells to the total number of counted cells (mitotic index±S.D.) [23].

Quantification of polymeric and depolymerised tubulin fractions

To assess early effects on the microtubule cytoskeleton, 518A2 cells cultured for 24 h in 24-well plates (5×10^4 cells/well) were exposed to DMSO (control), CA-4 as a positive control (1 μM), or increasing concentrations of the imidazoles **3** and **6** (50, 100, 250, 500, 1000 nM) for 6 h. The cells were then harvested by trypsination and centrifuged at 400 g for 5 min at room temperature. The resulting cell pellet was resuspended in 100 μL hypotonic cell lysis buffer (20 mM Tris-HCl, 1 mM $MgCl_2$, 2 mM EGTA, 0.5 % Triton X-100, pH 6.8) supplemented with protease inhibitor (protease inhibitor cocktail Set III, EDTA-free, Calbiochem) for 10 min at room temperature. After centrifugation at 12,000 g (10 min, room temperature), the supernatant containing soluble, depolymerised tubulin was separated from the pellet fraction representing detergent-insoluble, polymeric microtubules [23, 24]. Cell lysate and the pellet fractions were mixed with 100 μL 2× SDS-sample buffer (4 % SDS, 20 % glycerol, 20 mM DTT, 0.005 % bromophenol blue in 125 mM Tris-HCl, pH 6.8) and boiled at 95 °C for 10 min. Equal volumes of the samples were subjected to 10 % SDS-polyacrylamide gel electrophoresis followed by a standard Western blotting procedure and chemiluminescent detection (anti-alpha-tubulin mouse monoclonal antibody, clone no. TU-01, ca. One microgram per milliliter; goat anti-mouse IgG-HRP conjugate, Cell Signaling Technology) of the alpha-tubulin content. ImageJ software was used for graphical work and densitometric analyses.

Fluorescence labelling of microtubules, actin filaments and focal adhesions

Cells were seeded on glass coverslips (5×10^4 518A2 cells/well, 1×10^5 HUVECs/well) and allowed to adhere for 24 h and then treated with vehicle (DMSO) or various concentrations of CA-4 or the imidazoles **3**, **6**, or **7**. After 24 h of incubation cells were fixed with 4 % formaldehyde in PBS for 20 min at room temperature followed by blocking and permeabilisation (1 % BSA, 0.1 % Triton X-100 in PBS) for 30 min. For visualisation of filamentous actin (F-actin) coverslips were incubated with 1 U AlexaFluor®-488-conjugated phalloidin (Invitrogen) for 1 h at 37 °C. For immunostaining of microtubules and paxillin-associated focal adhesions fixed and permeabilised cells were treated with a primary antibody against alpha-tubulin (anti-alpha-tubulin, mouse monoclonal antibody, clone no. TU-01, ca. 10 μg/mL) or against paxillin (anti-paxillin, mouse monoclonal antibody, clone no. 177/Paxillin, 0.5 μg/mL, BD Transduction Laboratories) followed

by incubation with a secondary antibody conjugated to AlexaFluor®-488 (goat anti-mouse IgG-AlexaFluor®-488 conjugate, Cell Signaling Technology) for 1 h in the dark. Coverslips were mounted in Mowiol 4-88-based mounting medium containing 2.5 % (w/v) DABCO and 1 μg/mL DAPI for counterstaining the nuclei. Cytoskeletal components were documented by fluorescence microscopy (ZEISS Axio Imager.A1; 400× magnification for microtubule and microfilament staining, 630× for paxillin staining).

Tube formation assay with endothelial cells

The ability of permanent Ea.hy926 endothelial hybrid cells to form vascular-like networks upon growth factor stimulation was used to assess the vascular-disruptive activity of CA-4, **3** and **6** in vitro. Ea.hy926 cells retain essential endothelial characteristics and are an appropriate, often used model for angiogenesis studies [25, 26]. In the so-called tube formation assay Ea.hy926 cells (5×10^4/well) were grown for 12 h on thin Matrigel™ (basement membrane matrix, high concentration, with growth factors, BD Biosciences) layers pre-gelled in the wells of a black 96-well cell culture plate (20 μL of pure matrigel solution, 30 min at 37 °C) and then treated with vehicle (DMSO), CA-4 or the compounds **3** or **6** (50 nM). Tubular networks were documented by light microscopy (100× magnification, Axiovert 135, AxioCam MRc 5, ZEISS) after a further 12 h incubation. To exclude false-positive effects of contractile cells and tubule disruption as a consequence of the cytotoxicity of the compounds rather than early cytoskeletal rearrangements, MTT was additionally added to each well (25 μL 0.5 % MTT solution in PBS). After incubation for 2 h at 37 °C the plates were centrifuged (300 g, 4 °C, 5 min) and the supernatant was carefully aspirated. The cells were lysed and the precipitated formazan was redissolved by adding 100 μL of an SDS-DMSO solution (10 % SDS, 0.6 % acetic acid in DMSO) to each well. The absorbance at wavelengths 570 and 630 nm (background) was measured using an automatic ELISA microplate reader (Tecan) and the percentage of viable cells was calculated relative to controls.

Chorioallantoic membrane (CAM) assay with fertilised chicken eggs [27]

Chicken eggs (SPF eggs, VALO Biomedia) were incubated (37 °C, 50–60 % humidity) until day 7 after fertilisation and opened by cutting a window of 2–3 cm diameter into the pole end of the eggshell. Rings of silicon foil (5 mm diameter) were placed on the developing vessels within the CAM and the windows were sealed with tape followed by further incubation for 24 h. Dilutions of DMSO (control) and the imidazoles **3** and **6** in PBS were pipetted inside the silicon ring (10 μL of a 25 or 50 μM dilution) and alterations in the blood vessel organisation were documented after 0 and 24 h post application with a stereomicroscope (60× magnification, Traveller).

Animal studies

The vascular-disrupting activity of **6** was studied on the established model of highly vascularised 1411HP xenograft tumours previously described [18]. This study was approved by the Laboratory Animal Care Committee of Sachsen-Anhalt, Germany. Nude mice (Harlan and Winkelmann, Borchen, Germany) received 30 mg/kg body weight of compound **6** by intraperitoneal injection and tumour discoloration was documented after 24 h with a Canon IXUS 50. For histological examination the tumours were explanted, fixed in 4 % formalin, and embedded in paraffin. Hematoxylin/eosin (HE) staining of the tissue slices was performed according to standard protocols. HE images shown are representative of three independent in vivo observations.

Matrigel-based transwell migration assay

This assay provides a realistic three-dimensional model for tumour cell invasion stimulated by a chemoattractant. It takes into account both degradation and active movement of cells through a basement membrane matrix [28, 29]. The migration chambers were set up using ThinCert™ cell culture inserts with porous membranes (translucent PET membrane, 8 μm pore size, Greiner bio-one) for 24-well plates. The procedure for quantification of invasive cells was adapted from the manufacturer's application manual (ThinCert™ application notes, Greiner bio-one) with some alterations [30]. In brief, highly metastatic 518A2 melanoma cells were starved in serum-free DMEM for 24 h and harvested directly before seeding them into Matrigel™-coated (50 μL 1:1-dilution of Matrigel™ basement membrane matrix in serum-free DMEM, 30 min at 37 °C, 5 % CO_2, 95 % humidity; BD Biosiences) cell culture inserts (2×10^5 cells in 200 μL serum-free DMEM/insert) that were placed in the receiver wells filled with 600 μL DMEM containing 10 % FBS. Cells were exposed to DMSO (vehicle) or imidazole **6** at a final concentration of 10 or 50 nM for 48 h. The medium was removed from each well of the 24-well plate (lower compartment) and replaced with 500 μL 1× cell dissociation buffer (0.5 mM EDTA, 0.1 % sodium citrate in PBS, pH 7.4) containing 1 μM calcein-AM (calcein acetoxymethyl ester; non-fluorescent, cell-permeable dye). The plates with the inserts were incubated for 30 min at 37 °C for both sufficient detachment of the cells from the membrane underside or the surface of the bottom well and conversion of intracellular calcein-AM into the membrane-impermeable fluorescent calcein. The ThinCerts™ were then discarded and the cell suspension containing only invasive cells was transferred to the wells of a black 96-well plate. Migratory cells were quantified with a microplate reader (Tecan) by measuring the

calcein fluorescence (excitation/emission wavelength: 485 nm/520 nm) that was calculated as percentage of that of DMSO-treated control cells set to 100 %.

Trans-endothelium migration assay

Hanging cell culture inserts were used to build upper and lower compartments separated by an artificial endothelium which was constituted by a basement membrane matrix and a confluent endothelial monolayer [31–33]. Briefly, Ea.hy926 endothelial cells (1×10^5 cells in 50 μL DMEM) were seeded onto the underside of an insert membrane (24-well plate inserts, translucent PET membrane, 3.0 μm pore size, greiner bio-one) and allowed to adhere for 24 h after placing the inserts upside down into humidified wells of a 6-well plate. The inner membrane of the inserts was sealed with a thin Matrigel™-layer (20 μL 1:1-dilution in serum-free DMEM, gelled for 30 min at 37 °C, 5 % CO_2, 95 % humidity; BD Biosiences) and covered with 200 μL serum-free DMEM. The inserts were placed in the wells of a 24-well plate with 600 μL DMEM containing 10 % FBS and incubated for additional 24 h to get a confluent Ea.hy926 monolayer [34]. 518A2 cells confluently grown in cell culture dishes were starved in serum-free DMEM for 24 h prior to labelling with the carbocyanine dye DiI according to the manufacturer's instructions (15 min, 37 °C, 5 μL Vybrant™ DiI Cell-Labeling Solution per 1×10^6 cells/mL serum-free medium, Molecular Probes®, life technologies). Then the medium in the inserts was discarded and 200 μL of the DiI-stained 518A2 cell suspension in serum-free DMEM (10,000 cells/insert) were pipetted to each insert. The cells were allowed to adhere overnight and incubated with non-toxic concentrations of Et-brimamin **6** (10 or 50 nM). After 48 h the medium from the inserts and the receiver wells was removed and cells on the upper side of the insert were scraped off with a cotton swab [34]. For qualitative analyses cells on the membrane underside were fixed (4 % formaldehyde in PBS, 30 min, rt), washed with PBS and mounted in Mowiol 4-88-based mounting medium with 1 μg/mL DAPI for fluorescence microscopy. For quantification of invasive cells 500 μL 1× cell dissociation buffer (0.5 mM EDTA, 0.1 % sodium citrate in PBS, pH 7.4) containing 1 μM calcein-AM were added to the wells and the plates were incubated for 30 min at 37 °C for cell detachment and calcein-AM conversion. The cell suspension containing calcein-stained endothelial cells and red-fluorescent invasive tumour cells was transferred to the wells of a black 96-well plate and analysed for their calcein (excitation/emission wavelength: 485 nm/520 nm) and DiI (excitation/emission wavelength: 550 nm/570 nm) fluorescence with a microplate reader (Tecan). The green or red fluorescence intensity of DMSO-treated control cells was set to 100 %. The ratio of red to green fluorescence intensities was taken as a measure for the percentage of trans-endothelium-migrated 518A2 cells with respect to DMSO controls and the total number of viable cells.

Results and discussion

Table 1 summarises the IC_{50} values of reference compounds and the new CA-4 analogous imidazoles in MTT cytotoxicity assays. All new compounds were first tested against the CA-4-sensitive 518A2 melanoma and the CA-4-resistant HT-29 colon carcinoma cell lines. Despite its shortcomings when applied in vivo CA-4 exhibits a great in vitro cytotoxicity with nanomolar IC_{50} values against many cancer cell lines. However, it is far less efficacious against HT-29 cells which discharge it quickly by means of their ABC (ATP-binding cassette) transporters [21]. The imidazole analogue **1** was previously shown to be efficacious against HT-29 cells, and even more so the closely related analogues **3** ('brimamin', *N*-methyl-4-(3-bromo-4,5-dimethoxyphenyl)-5-(3-amino-4-methoxyphenyl)-imidazole) and **9** that bear a *meta*-halo substituted A-ring and a *meta*-amino-*para*-methoxyphenyl B-ring [17, 18].

We now found that keeping the *meta*-bromo or -chloro substituent at the A-ring and the *meta*-amino substituent at the B-ring while replacing the *para*-methoxy group on the B-ring by an ethoxy residue led to a further increase of the cytotoxicity against both the CA-4 sensitive and resistant cell lines. For instance, the B-*meta*-amino derivatives **6** and **11** were twice as efficacious as **3** or **9**, respectively. The B-*meta*-fluoro (**7**, **12**) or B-*meta*-chloro (**8**) derivatives were even nearly ten times more efficacious than **4**, **10**, or **5**, respectively. Most active were the first generation *para*-methoxy derivative 'brimamin' (**3**), its new ethoxy congener **6** ('Et-brimamin'), and 'Et-brimfluor' **7**, the *meta*-fluoro analogue of **6**. They all displayed two-digit nanomolar IC_{50} (72 h) values against cells of 518A2 melanoma, HT-29 and HCT-116 colon carcinoma, and multidrug-resistant MCF-7/Topo breast carcinoma. CA-4 and the derivatives **3**, **6**, and **7** also inhibited the growth of Ea.hy926 hybrid endothelial cells and primary human umbilical vein endothelial cells (HUVEC) in MTT assays with IC_{50} in the lower nanomolar range. However, the compounds showed a distinct selectivity for cancer and endothelial cell lines over nonmalignant fibroblasts (CHF) which were hardly affected even at concentrations of 10 μM.

CA-4 analogous imidazoles induce mitotic cell cycle arrest

518A2 melanoma and HT-29 colon carcinoma cells were treated for 24 h with equitoxic concentrations of CA-4 or the imidazoles **3** or **6** and subjected to flow cytometric cell cycle analyses (Fig. 2). In the case of 518A2 cells a decrease of cells with G1 DNA content was found together with a slightly increased G2-M population and a significantly higher

Table 1 In vitro cytotoxicity of CA-4 and imidazoles **1**–**12** against 518A2 melanoma, HT-29 and HCT-116 colon, MCF-7/Topo breast carcinoma cells, the endothelial hybrid cell line Ea.hy926, HUVEC, and nonmalignant chicken heart fibroblasts (CHF)

	Cell lines						
	518A2	HT-29	HCT-116	MCF-7/Topo	Ea.hy926	HUVEC	CHF
CA-4	1.8±0.1	>5000	2.6±0.2	154±33	11±2	1.2±0.1	>5000
1	>100,000 [a]	64±14 [a]	n.d.	>10,000 [a]	n.d. [b]	n.d.	n.d.
2	61±1	>1000	215±17	n.d.	n.d.	n.d.	n.d.
3	29±2	15±1	27±2	100±9	28±4	23±7	>10,000
4	184±5	305±59	249±29	236±25	n.d.	n.d.	n.d.
5	2429±46	>5000	n.d.	n.d.	n.d.	n.d.	n.d.
6	14±2	6.9±1.2	5.1±0.4	72±6	15±2	14±4	>10,000
7	27±5	38±1	177±8	97±12	140±4	n.d.	>10,000
8	249±14	588±11	n.d.	n.d.	n.d.	n.d.	n.d.
9	48±3	40±1	n.d.	n.d.	n.d.	n.d.	n.d.
10	400±100[a]	530±30[a]	n.d.	n.d.	n.d.	n.d.	n.d.
11	22±2	38±4	n.d.	n.d.	n.d.	n.d.	>50,000
12	28±1	50±1	189±8	n.d.	n.d.	n.d.	>10,000

[a] Values from an earlier publication used for reference compounds [18]

[b] Not determined

IC_{50} [nM] values after 72 h exposure as the mean of three independent MTT assays±S.D

percentage of sub-diploid, apoptotic cells. The magnitude of these cell cycle alterations correlated well with the IC_{50} values found for CA-4, **3** and **6** (cf. electronic supplementary material, Tables S1, S2). The sensitivity of 518A2 cells to CA-4 and the imidazoles **3** and **6** might be due to their high proliferation rate. Treatment of CA-4-resistant HT-29 cells with 100 nM **3** or **6** led to a significant accumulation of cells in the G2-M phase which is typical of antimitotic compounds. The number of apoptotic events was only slightly increased, probably since 24 h are too short an incubation period for these cells to enter into apoptosis as a consequence of prolonged mitotic arrest [9, 35].

We substantiated these results by fluorescence microscopy of DAPI-stained nuclei of cancer cells treated with CA-4, **3** or **6** in order to differentiate between cells in G2 phase and mitotic cells based on the chromatin organisation. After 6 h incubation with appropriate concentrations the number of mitotic cells increased markedly (Table 2). The mitotic index, which was about 9 % for DMSO-treated control cells of either cell line, was significantly shifted to 40 or 32 %, respectively, of cells with condensed DNA upon stimulation with CA-4 and to more than 40 % upon exposure to brimamin (**3**) or Et-brimamin (**6**). Due to their CA-4 resistance a higher dose of 5 μM CA-4 was required to achieve accumulation of mitotic cells to an extent comparable to that caused by 100 nM of **6** (Fig. 3).

Imidazoles **3** and **6** disrupt microtubules and induce cytoskeletal reorganisation

Tubulin-binding agents interfere with the microtubule dynamics eventually blocking mitotic progression and cell division. Thus, we investigated the effects of the new *N*-methyl-4,5-diarylimidazoles on microtubule organisation and the cytoskeletal response in cancer and endothelial cells. First, we compared brimamin (**3**), Et-brimamin (**6**), and Et-brimfluor (**7**) for their efficiency in suppressing tubulin polymerisation in vitro. In 518A2 cells treated for 3 h with increasing concentrations of **3**, **6** or **7** initially intact microtubules were destructed in a concentration-dependent manner (Fig. 4). Exposure to Et-brimamin (**6**), the compound with the lowest IC_{50} (72 h) value at this cell line, induced complete disruption even at a concentration of 250 nM. In contrast, 250 nM of brimamin (**3**) or Et-brimfluor (**7**) eroded the highly organised microtubular network but left some coherent clusters of intact microtubules. Apparently, the cytotoxicity of the tested imidazoles correlates well with their ability to disrupt microtubules. This was further corroborated by quantifying the fraction of intact microtubules in treated 518A2 cells (Fig. 5).

Disruption of microtubular dynamics results in higher cellular levels of free tubulin heterodimers that are part of the detergent-soluble supernatant of cell lysates and that can be separated from intact tubulin polymers by centrifugation. As shown by Western blot analyses of the insoluble pellet fraction, microtubule disruption is induced by Et-brimamin (**6**) at lower concentrations than those required of brimamin (**3**) for the same effect. This might be due to a higher affinity of **6** for tubulin. In line with this is the greater inhibitory effect of **6** on the polymerisation of purified tubulin in a cell-free assay when compared with the effects by the less cytotoxic analogues brimfluor (**4**) or **1** (cf. electronic supplementary material, Table S4). Thus, the tubulin binding capacity of the imidazoles correlates well with their cytotoxicity against cancer cells.

Next, we investigated the cellular actin stress fibre formation as a typical response to tubulin-binding agents. Since changes in the cellular contractility upon actin stress fibre development play an important role for the antivascular

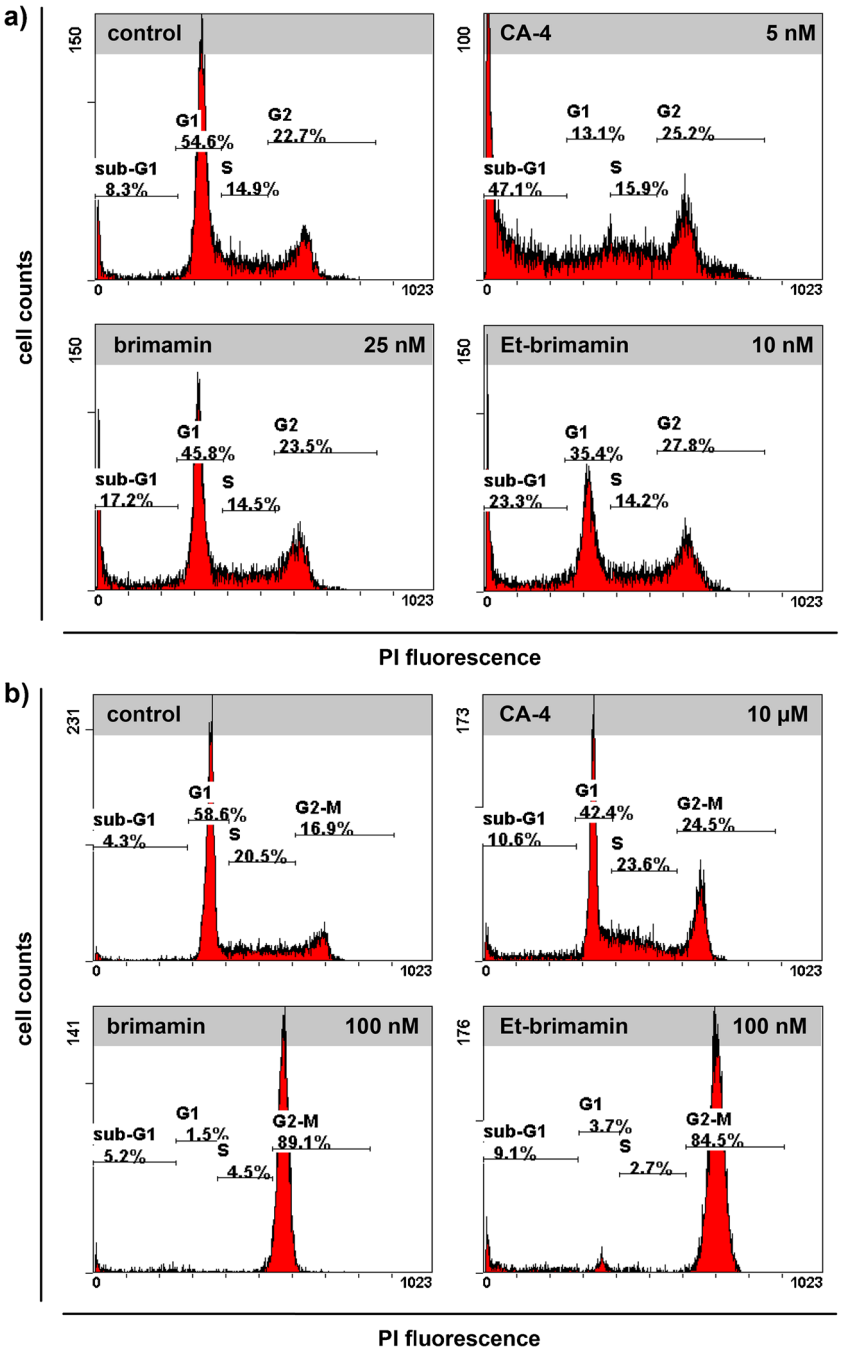

Fig. 2 Effect of CA-4, brimamin **3**, and Et-brimamin **6** on the cancer cell cycle. Effect on the cell cycle of (**a**) CA-4-sensitive 518A2 melanoma and (**b**) CA-4-resistant HT-29 colon carcinoma cells after 24 h exposure. Typical cell cycle profiles and percentage of treated cells in G1, S and G2-M phase as well as sub-G1 events (apoptotic cells) as obtained by flow cytometry after DNA staining with propidium iodide (PI)

Table 2 Percentage of mitotic cells (%) in cultures of 518A2 melanoma or HT-29 colon carcinoma cells treated with CA-4 (518A2: 5 nM, HT-29: 5 µM) or with imidazoles **3** or **6** (100 nM) for 6 h

	Control	CA-4	Brimamin 3	Et-brimamin 6
518A2	9.4±0.6	39.7±2.4	46.4±3.6	52.2±6.8
HT-29	8.9±1.7	31.7±3.4	41.2±3.8	39.2±3.2

Data obtained from counting DAPI-stained nuclei of at least 800 cells and represented as mean±SD, control: DMSO

activity of CA-4 we used primary endothelial cells (HUVEC) for these experiments. In response to exposure to CA-4 or the most active imidazole **6** HUVEC displayed a dense network of actin stress fibres when compared to DMSO-treated control cells (Fig. 6).

Stress fibre formation was associated with an increase in focal adhesions as visualised by immunofluorescent staining of focal adhesion-associated paxillin. Both processes are mediated by Rho which gets activated upon perturbation of the tubulin cytoskeleton. Eventually, they lead to an increase in cell-matrix contacts and in cell contractility [36, 37]. Given

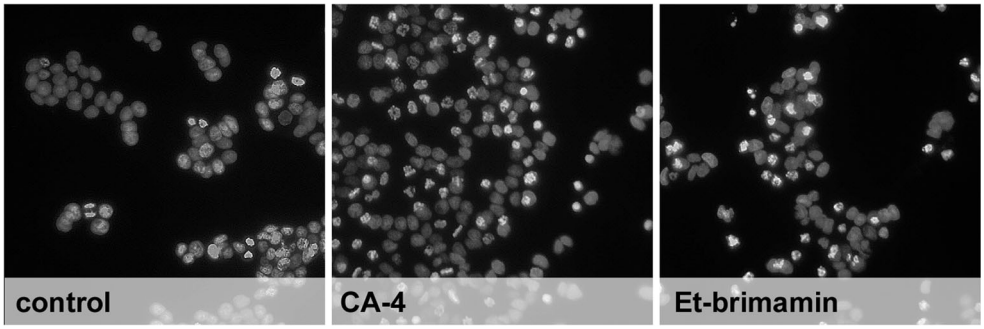

Fig. 3 Accumulation of mitotic HT-29 colon carcinoma cells. Accumulation of mitotic HT-29 colon carcinoma cells after exposure to CA-4 (5 μM) or Et-brimamin **6** (100 nM) for 6 h. Nuclei stained with DAPI (200-fold magnification)

that a balanced dynamics and assembly of microfilaments and focal adhesions is required for endothelial cell-matrix interactions and the endothelium stability [37] it is understandable that CA-4 and Et-brimamin (**6**) are likely to show some antimigratory and antivascular activity by inducing a defective focal adhesion turnover.

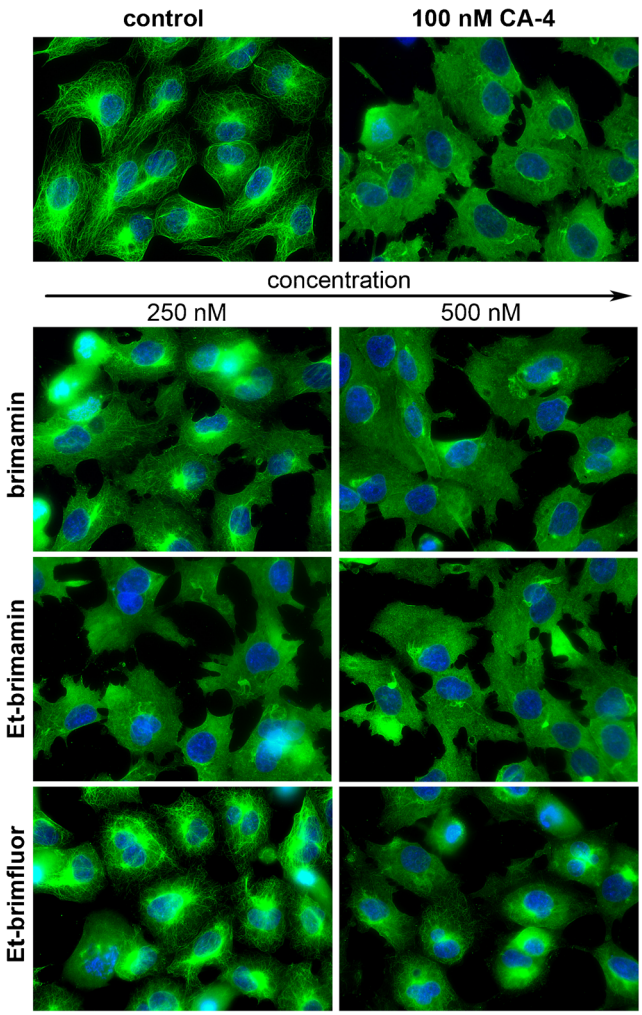

Fig. 4 Effects of CA-4 and of brimamin (**3**), Et-brimamin (**6**) and Et-brimfluor (**7**) on the microtubule organisation in 518A2 melanoma cells. Effects after 3 h incubation. Immunofluorescent labelling of alpha-tubulin (green), nuclei (blue) counterstained with DAPI (400-fold magnification)

CA-4, brimamin (**3**), and Et-brimamin (**6**) are antivascular in vitro and in vivo

The antivascular potential of the imidazoles **3** and **6** was first tested in vitro by means of the so-called tube formation assay. Endothelial cells such as HUVEC and the more often used hybrid Ea.hy926 cells differentiate into tubular, vessel-like networks upon stimulation by growth factors contained in a thin Matrigel layer that serves as a cell adhesion surface [25, 26]. We exposed preformed Ea.hy926 cell networks for 12 h to non-toxic concentrations of CA-4, brimamin (**3**) or Et-brimamin (**6**). Figure 7 shows the resulting disruption of established tubes and branches caused by the retraction of individual cells which is a good indication of a potential antivascular effect by the test compounds in vivo.

Endothelial cell migration and differentiation are essential steps in blood vessel maturation which may get stuck, though, in case of severe cytoskeletal alterations [3, 5, 37]. Since we can exclude any significant contribution by the cytotoxic component of the test compounds **3** and **6** after so short a time (viable cells after 12 h exposure to brimamin **3**: 94.9 %±3.9 % and to Et-brimamin **6**: 83.7 %±2.4 % with respect to DMSO-treated controls set to 100 %) we asume that the destruction of tubular endothelial cell networks is the result of early drug-induced cytoskeletal reorganisations leading to a breakdown of cell-cell adhesion and a loss of the stretched morphology of individual cells.

The vascular-disrupting activity of imidazoles **3** and **6** was also demonstrated in vivo by their impact on the blood vessel system of fertilised chicken eggs (Fig. 8a). After topical application of non-lethal doses onto the vascularised chorioallantoic membrane (CAM) existing blood vessels became leaky and small branches were completely distroyed with hemorrhages appearing. Though CA-4 was the most effective compound in these CAM assays doses beyond 2.5 nmol of it frequently killed the chicken embryos. In contrast, doses of 5 nmol brimamin (**3**) or of 2.5 nmol Et-brimamin (**6**) were tolerated well while showing comparable vascular-disrupting effects.

We also investigated the vascular-disrupting activity of **6** in highly vascularised xenografts of the 1411HP germ

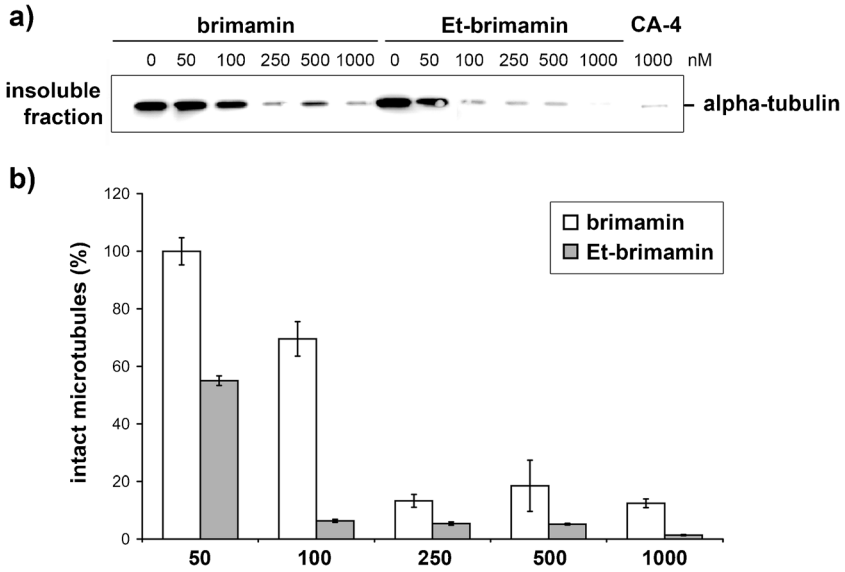

Fig. 5 Brimamin (**3**) and Et-brimamin (**6**) decrease the levels of tubulin polymers in 518A2 cells. **a**) Detergent-insoluble fractions of lysates from 518A2 melanoma cells, treated for 6 h with various concentrations of CA-4, **3** or **6**, were subjected to SDS-PAGE and the content of tubulin was visualised by immunoblotting for alpha-tubulin (55 kDa). **b**) The concentration-dependent (50–1000 nM) levels of tubulin polymers in insoluble cell lysate fractions (intact microtubules) quantified by densitometric analyses of Western blots obtained from two independent experiments, means±S.D

cell tumour cell line which were previously used as an established animal model for the test of VDA [18]. A single treatment of the xenograft bearing mice with 30 mg/kg of **6** induced a distinct tumour discoloration due to intratumoural haemorrhage (Fig. 8b). Histological examination of the treated tumour revealed features typically observed after treatment with CA-4P or other vascular-disrupting agents [5, 13] such as extensive central necrosis and a remaining thin rim of surviving tumour cells (Fig. 8c). Signs of toxicity such as a significant loss of weight were only observed in mice treated with single doses exceeding 60 mg/kg body weight.

To prove the efficacy of the new imidazoles also in CA-4 resistant tumours we undertook preliminary xenograft studies with HT-29 tumours which are far less vascularised and more slowly growing than 1411HP tumours. Here, we observed a significant reduction of the tumour growth in the treated mice (cf. electronic supplementary material, Figure S1) which nicely mirrors the capability of Et-brimamin (**6**) to overcome the CA-4 resistance of HT-29 cells in vitro (cf. Table 1). Although

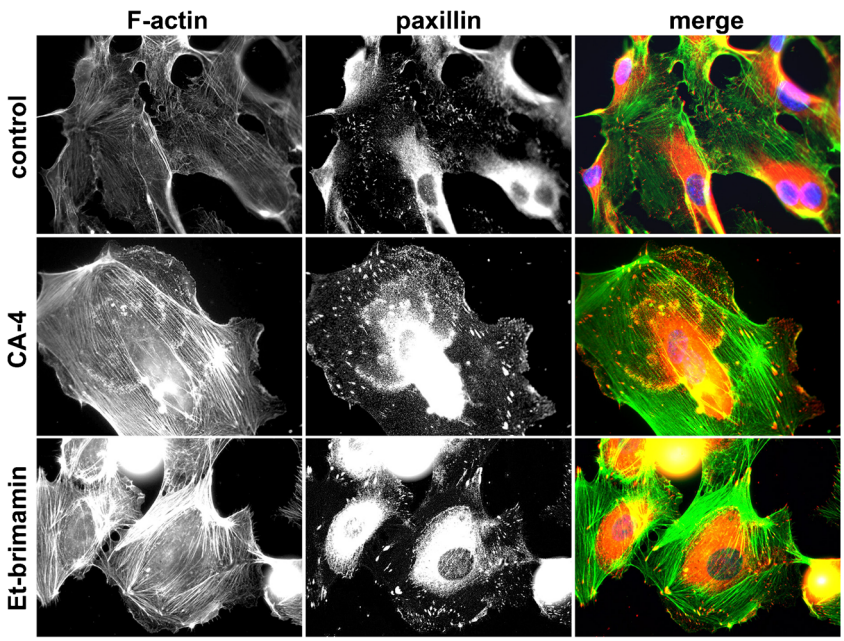

Fig. 6 Effect of CA-4 and Et-brimamin (**6**) on the cytoskeletal organisation of primary endothelial cells (HUVEC). Effect of CA-4 (10 nM, 24 h) and Et-brimamin (**6**) (50 nM, 24 h) on the cytoskeletal organisation of human umbilical vein endothelial cells. Fluorescence labelling of filamentous actin (F-actin, *green*) and paxillin-associated focal adhesions (*red*). Nuclei (*blue*, merge) counterstained with DAPI (630-fold magnification)

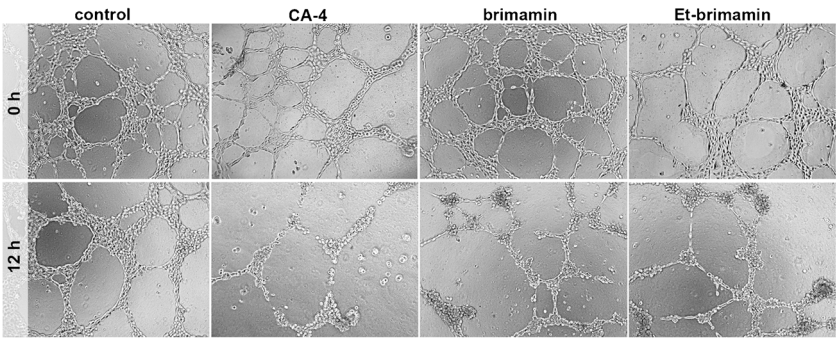

Fig. 7 Tube formation by Ea.hy926 endothelial cells grown on Matrigel. Cells were treated for 12 h with 50 nM CA-4, brimamin **3** or Et-brimamin **6** (100-fold magnification)

this has to be confirmed in a larger trial these findings recommend **6** as a promising drug candidate for the treatment of CA-4-resistant tumours. It also underlines that a strong direct tumour cell cytotoxicity is an important component of the overall activity of **6** against solid tumours, and very likely of other related imidazoles as well.

Et-brimamin (**6**) shows antimetastatic activity in in vitro metastasis models

Neo-vascularisation/angiogenesis is also the initial step in the cascade of processes eventually leading to the metastasis of tumours [28, 31, 38, 39]. Since the subcellular organisation and the dynamic turnover of microtubules, microfilaments, and focal adhesion are essential to angiogenesis- and metastasis-related cell migration, disturbing the balance of these processes might not only affect blood vessel integrity but also the migratory behaviour of prometastatic tumour cells. We assessed the most active imidazole **6** for such effects employing an in vitro model based on a modified Boyden two-chamber system where cells migrate to a lower compartment that is separated by a porous membrane and a Matrigel layer as a surrogate of the natural extracellular matrix (ECM) [29, 30, 40]. This assay provides a realistic three-dimensional model for tumour cell invasion that takes into account both the degradation of a basement membrane matrix and the active

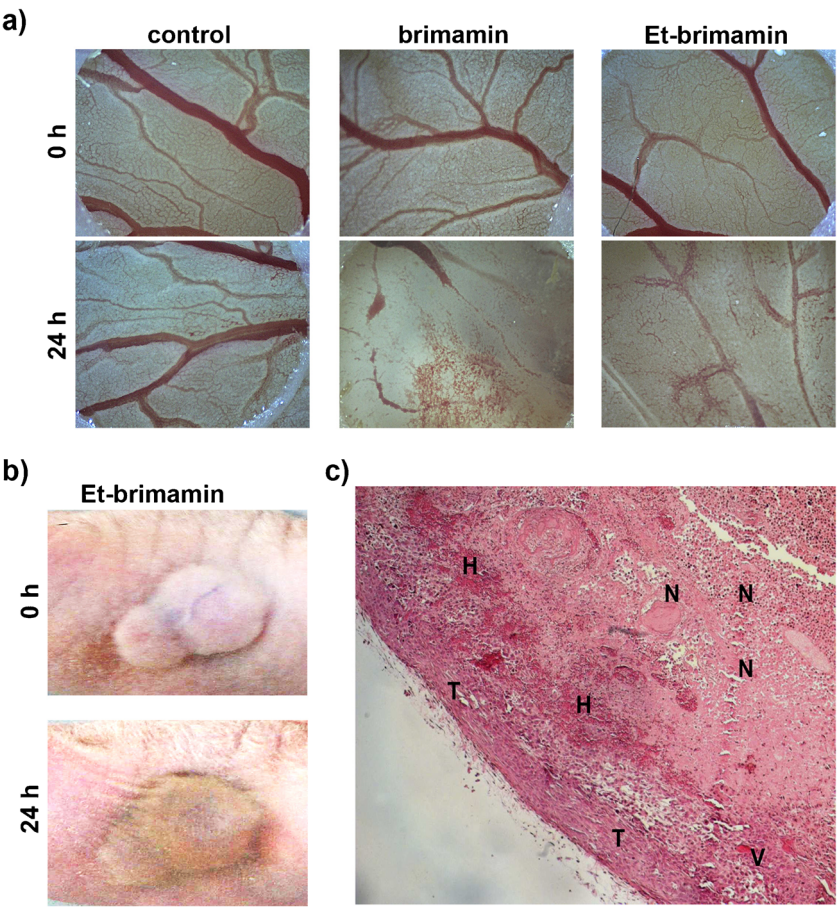

Fig. 8 Vascular-disrupting effects of brimamin (**3**) and Et-brimamin (**6**) in vivo. **a**) Effects by **3** (5 nmol) and **6** (2.5 nmol) on blood vessels in the chorioallantoic membrane (CAM) of fertilised chicken eggs (60-fold magnification). **b**) I.p. administration of **6** (30 mg/kg body weight) to a mouse bearing a 1411HP germ cell tumour xenograft leads to tumour discoloration due to haemorrhages. **c**) Lateral section of the tumour shown in **b**) (*bottom*, *left*) after HE staining featuring a large necrotic core area (N) and haemorrhages (H) surrounded by a cortical layer of vital tumour cells (T) which encompasses residual intact blood vessels (V)

movement of cells through this ECM (Fig. 9, top left) [29, 30, 40]. Directional movement towards the lower compartment was stimulated by providing FBS as a chemoattractant to tumour cells that had been starved overnight. In addition, we also employed a transwell migration assay that mimics the situation of tumour cell intravasation during metastasis by imposing an additional barrier between two compartments in the form of an endothelial cell monolayer [31–33]. This assay emulates the crucial part of the metastatic process when tumour cells enter the vasculature or penetrate the endothelium [31–33]. Once more, hanging cell culture inserts were employed for building an upper and lower compartment separated by an artificial endothelium which was constituted by a basement membrane matrix and a dense, confluent endothelial monolayer (Fig. 9, top right). Highly invasive 518A2 melanoma cells that had migrated through the ECM layer and successfully crossed the endothelium could be discriminated from endothelial cells by a preceding staining of all 518A2 cells with the non-toxic permanent dye DiI [41, 42]. All cells found in the lower compartment or at the underside of the insert membrane were detached and stained with calcein-AM. The number of invasive 518A2 cells was ascertained by measuring the calcein fluorescence intensity (transwell migration, Table 3) or the ratio of red fluorescent, DiI pre-stained 518A2 cells (only invasive 518A2 cells) to all green (calcein) fluorescent cells (endothelial and invasive 518A2 cells; trans-endothelium migration, Table 3; cf. Electronic supplementary material for original fluorescence ratios, Table S6).

Table 3 Migration of 518A2 melanoma cells through Matrigel-coated inserts (transwell migration) or a confluent endothelial cell monolayer grown on inserts (trans-endothelium migration) when exposed to vehicle or Et-brimamin **6** for 48 h

Invasive cells (%)	Control	10 nM Et-brimamin	50 nM Et-brimamin
Transwell migration	100±0.7	53.4±4.6	49.6±2.4
Trans-endothelium migration	100±2.9	73.0±2.5	69.5±4.1

Percentage of invasive cells (%) derived from intracellular calcein fluorescence relative to DMSO-treated controls. Data represent mean±SD from two independent experiments

The concentrations of Et-brimamin (**6**) used in both invasion assays (10, 50 nM) with highly invasive 518A2 melanoma cells [43, 44] were shown to be virtually non-toxic by TUNEL [TdT (terminal desoxynucleotide transferase)-mediated dUTP nick end labelling]-detection of DNA fragmentation (apoptotic cells) after 48 h (cf. electronic Supplementary material, Fig. S2, Table S5 and description of the method). Imidazole **6** suppressed the chemoattractant-stimulated migration through Matrigel-coated membranes to about 50 %

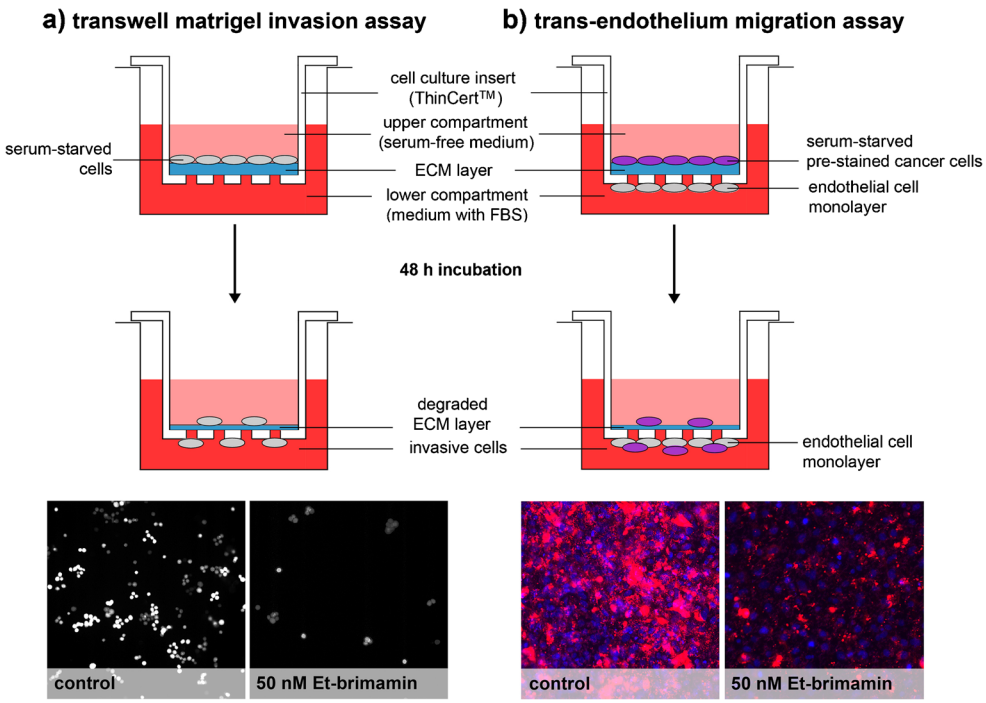

Fig. 9 Antimetastatic activity of Et-brimamin n on highly invasive 518A2 melanoma cells in transwell migration assays. *Upper panel*: schematic representation of two three-dimensional in vitro assays for the quantification of the metastatic potential of 518A2 melanoma cells, based on the ThinCert™product sheet by greiner bio-one. *Lower panel*: *left*: fluorescence micrographs of 518A2 cells on the insert membrane after calcein staining (100-fold magnification) in a transwell matrigel invasion assay; *right*: fluorescence micrographs of the coating on the underside of the insert membrane with 518A2 cells highlighted by the red DiI fluorescence (nuclei counterstained with DAPI, *blue*; 400-fold magnification) in a trans-endothelium migration assay

(Table 3, Fig. 9, bottom left). Migration of 518A2 cells through both the basement membrane matrix and a tight endothelial cell monolayer was distinctly impaired by 10 nM Et-brimamin (**6**), a concentration that hardly affected the total number of viable cells (cf. electronic supplementary material, Table S5). Application of 50 nM **6** inhibited the cell growth as detected by the calcein fluorescence of cells within the lower compartments to 70 % of the control with concomitant halving of cell invasion as assessed from their red DiI membrane fluorescence. In summary, the administration of non- or slightly toxic concentrations of **6** resulted in a reduction of transendothelial invasion/intravasation to ca. Seventy percent (Table 3, Fig. 9, bottom right).

From the reduced numbers of invasive cells we conclude that exposure to Et-brimamin (**6**) induced an extensive cytoskeletal rearrangement which is responsible for the impairment of directional 3D-migration and of squeezing through constrictions such as endothelial cell-cell interfaces or the micropores of the ThinCert™ inserts.

Conclusions

When compared to the first generation of *N*-methyl-4-aryl-5-(4-methoxyphenyl)imidazoles, the analogues bearing a *para*-ethoxy residue at the B-ring generally exhibited stronger effects on the microtubular and actin cytoskeletons of cancer and endothelial cells and on their viability and propensity to migrate or form blood vessel-like tubular structures. In contrast, a replacement of the *meta*-amino group on the B-ring by a halide had a detrimental effect in both series of imidazoles, most pronounced for the couples **3**/**4** and **6**/**7**. Et-brimamin (**6**), the B-*para*-ethoxy congener of the best performing first generation imidazole, brimamin (**3**) [18], turned out to be the best compound of the current series regarding its in vitro inhibition of cancer and endothelial cell growth and its destructive impact on the microtubules. Like the lead CA-4 both analogues **3** and **6** displayed a pronounced vascular-disrupting activity in all its facets in vitro and in vivo. This originates from initial damages to the tubulin cytoskeleton which in turn lead to an adaptation of other cellular processes such as the formation of contractile actin-myosin stress fibres and of cell-matrix focal adhesions eventually resulting in the observed loss of the endothelium integrity [3, 5]. When compared with CA-4 the imidazoles **3** and **6** were far less toxic against the nonmalignant chicken heart fibroblasts in our panel and also against the chicken embryos in the CAM assay. Excellent antitumour activity in combination with merely marginal in vivo side effects in xenograft mouse models had already been reported for brimamin **3** [18]. Hence we are confident that cardiotoxicity as a typical side effect of other clinically used inhibitors of microtubule assembly [45] will play a minor role. The 3D-migration experiments of the current study proved that there is a link also between the cytoskeletal alterations caused by CA-4 and its imidazole analogues and their antimetastatic properties. Although there had been a good deal of evidence in literature for such a link [28, 31, 39, 47–50], the known inhibition of metastatic progression in vivo by CA-4 had been ascribed mainly to its inhibition of AKT function [46]. A tentative proposal for the mechanism of action of CA-4 as well as Et-brimamin (**6**) may be based on the observation that they enhanced the maturation of stable focal adhesions in primary endothelial cells (HUVEC). This effect should prevent the formation of the typical leading edges of migrating cells. So, hindered migration would be the consequence of the loss of cellular polarity which itself originates from the enormous cytoskeleton aberrations as demonstrated in our 3D in vitro metastasis models. Both of these models involve an artificial tumour microenvironment that cells need to get past by different motility or low adhesion mechanisms that cannot be detected by two-dimensional assays [28, 47, 49, 51, 52].

As to potential clinical applications of CA-4 derived imidazoles such as **6** it should be noted that the established strategy of starving solid tumours by blocking blood vessel formation via inhibition of VEGFR (vascular endothelial growth factor receptors) often leads to enhanced aggressiveness and resistance [52–54]. The combination of VEGFR inhibitors with antivascular and antimetastatic CA-4 derivatives, both at low doses, could reduce tumour angiogenesis and additionally prevent metastasis through cytoskeletal reorganisation. Further in vivo studies with metastatic cancers, including such obtained from actual patients under therapy, are currently underway.

Acknowledgments We are indebted to Dr. Florenz Sasse (Helmholtz Centre for Infection Research, Braunschweig, Germany) for assisting with fluorescence microscopy and to Franziska Reipsch (Department of Internal Medicine IV, Halle) for technical assistance.

Conflict of interest The authors declare that there are no conflicts of interest.

References

1. Pettit G, Singh S, Hamel E et al (1989) Isolation and structure of the strong cell growth and tubulin inhibitor combretastatin A-4. Experientia 45:209–211
2. Tron GC, Pirali T, Sorba G et al (2006) Medicinal chemistry of combretastatin A4: present and future directions. J Med Chem 49: 3033–3044. doi:10.1021/jm0512903
3. Kanthou C, Tozer GM (2007) Tumour targeting by microtubule-depolymerising vascular disrupting agents. Expert Opin Ther Targets 11:1443–1457. doi:10.1517/14728222.11.11.1443
4. Tozer GM, Kanthou C, Baguley BC (2005) Disrupting tumour blood vessels. Nat Rev Cancer 5:423–435. doi:10.1038/nrc1628
5. Kanthou C, Tozer GM (2009) Microtubule depolymerizing vascular disrupting agents: novel therapeutic agents for oncology and other

pathologies: microtubule depolymerizing vascular disrupting agents. Int J Exp Pathol 90:284–294. doi:10.1111/j.1365-2613.2009.00651.x
6. Nguyen TL, McGrath C, Hermone AR et al (2005) A common pharmacophore for a diverse set of colchicine site inhibitors using a structure-based approach. J Med Chem 48:6107–6116. doi:10.1021/jm050502t
7. Yamada HY, Gorbsky GJ (2006) Spindle checkpoint function and cellular sensitivity to antimitotic drugs. Mol Cancer Ther 5:2963–2969. doi:10.1158/1535-7163.MCT-06-0319
8. Bhalla KN (2003) Microtubule-targeted anticancer agents and apoptosis. Oncogene 22:9075–9086. doi:10.1038/sj.onc.1207233
9. Kanthou C, Greco O, Stratford A et al (2004) The tubulin-binding agent combretastatin A-4-phosphate arrests endothelial cells in mitosis and induces mitotic cell death. Am J Pathol 165:1401–1411
10. Kanthou C (2002) The tumor vascular targeting agent combretastatin A-4-phosphate induces reorganization of the actin cytoskeleton and early membrane blebbing in human endothelial cells. Blood 99:2060–2069. doi:10.1182/blood.V99.6.2060
11. Quan H, Xu Y, Lou L (2007) p38 MAPK, but not ERK1/2, is critically involved in the cytotoxicity of the novel vascular disrupting agent combretastatin A4. Int J Cancer 122:1730–1737. doi:10.1002/ijc.23262
12. Fan M, Du L, Stone A et al (2000) Modulation of mitogen-activated protein kinases and phosphorylation of Bcl-2 by vinblastine represent persistent forms of normal fluctuations at G2-M. Cancer Res 60:6403–6407
13. Lunt JS, Akerman S, Hill SA et al (2011) Vascular effects dominate solid tumor response to treatment with combretastatin A-4-phosphate. Int J Cancer 129:1979–1989. doi:10.1002/ijc.25848
14. Delmonte A, Sessa C (2009) AVE8062: a new combretastatin derivative vascular disrupting agent. Expert Opin Investig Drugs 18:1541–1548. doi:10.1517/13543780903213697
15. Del Conte G, Bahleda R, Morena V et al (2012) A phase I study of ombrabulin (O) combined with bevacizumab (B) in patients with advanced solid tumors. J Clin Oncol 30:(suppl); abstr 3080
16. Salmon HW, Siemann DW (2006) Effect of the second-generation vascular disrupting agent OXi4503 on tumor vascularity. Clin Cancer Res Off J Am Assoc Cancer Res 12:4090–4094. doi:10.1158/1078-0432.CCR-06-0163
17. Wang L, Woods KW, Li Q et al (2002) Potent, orally active heterocycle-based combretastatin A-4 analogues: synthesis, structure-activity relationship, pharmacokinetics, and in vivo antitumor activity evaluation. J Med Chem 45:1697–1711. doi:10.1021/jm010523x
18. Schobert R, Biersack B, Dietrich A et al (2010) 4-(3-Halo/amino-4,5-dimethoxyphenyl)-5-aryloxazoles and -*N*-methylimidazoles that are cytotoxic against combretastatin A resistant tumor cells and vascular disrupting in a cisplatin resistant germ cell tumor model. J Med Chem 53:6595–6602. doi:10.1021/jm100345r
19. Biersack B, Muthukumar Y, Schobert R, Sasse F (2011) Cytotoxic and antivascular 1-methyl-4-(3-fluoro-4-methoxyphenyl)-5-(halophenyl)-imidazoles. Bioorg Med Chem Lett 21:6270–6273. doi:10.1016/j.bmcl.2011.09.005
20. Bonezzi K, Taraboletti G, Borsotti P et al (2009) Vascular disrupting activity of tubulin-binding 1,5-diaryl-1H-imidazoles. J Med Chem 52:7906–7910. doi:10.1021/jm900968s
21. Schobert R, Effenberger-Neidnicht K, Biersack B (2011) Stable combretastatin A-4 analogues with sub-nanomolar efficacy against chemoresistant HT-29 cells. Int J Clin Pharmacol Ther 49:71–72
22. Biersack B, Effenberger K, Schobert R, Ocker M (2010) Oxazole-bridged combretastatin A4 analogues with improved anticancer properties. ChemMedChem 5:420–427. doi:10.1002/cmdc.200900477
23. Chang C-H, Yu F-Y, Wu T-S et al (2011) Mycotoxin citrinin induced cell cycle G2/M arrest and numerical chromosomal aberration associated with disruption of microtubule formation in human cells. Toxicol Sci 119:84–92. doi:10.1093/toxsci/kfq309
24. Lieuvin A, Labbé J-C, Dorée M, Job D (1994) Intrinsic microtubule stability in interphase cells. J Cell Biol 124:985–996
25. Aranda E, Owen GI (2009) A semi-quantitative assay to screen for angiogenic compounds and compounds with angiogenic potential using the EA. hy926 endothelial cell line. Biol Res 42:377–389
26. Bauer J, Margolis M, Schreiner C et al (1992) In vitro model of angiogenesis using a human endothelium-derived permanent cell line: contributions of induced gene expression, G-proteins, and integrins. J Cell Physiol 153:437–449
27. Nitzsche B, Gloesenkamp C, Schrader M et al (2010) Novel compounds with antiangiogenic and antiproliferative potency for growth control of testicular germ cell tumours. Br J Cancer 103:18–28. doi:10.1038/sj.bjc.6605725
28. Friedl P, Wolf K (2003) Tumour-cell invasion and migration: diversity and escape mechanisms. Nat Rev Cancer 3:362–374. doi:10.1038/nrc1075
29. Entschladen F, Drell TL, Lang K et al (2005) Analysis methods of human cell migration. Exp Cell Res 307:418–426. doi:10.1016/j.yexcr.2005.03.029
30. Albini A, Iwamoto Y, Kleinman HK et al (1987) A rapid in vitro assay for quantitating the invasive potential of tumor cells. Cancer Res 47:3239–3245
31. Geiger TR, Peeper DS (2009) Metastasis mechanisms. Biochim Biophys Acta Rev Cancer 1796:293–308. doi:10.1016/j.bbcan.2009.07.006
32. Li YH, Zhu C (1999) A modified Boyden chamber assay for tumor cell transendothelial migration in vitro. Clin Exp Metastasis 17:423–429
33. Okada T, Okuno H, Mitsui Y (1994) A novel in vitro assay system for transendothelial tumor cell invasion: significance of E-selectin and alpha 3 integrin in the transendothelial invasion by HT1080 fibrosarcoma cells. Clin Exp Metastasis 12:305–314
34. Laferriere J (2001) Transendothelial migration of colon carcinoma cells requires expression of E-selectin by endothelial cells and activation of stress-activated protein kinase-2 (SAPK2/p38) in the tumor cells. J Biol Chem 276:33762–33772. doi:10.1074/jbc.M008564200
35. Orth JD, Loewer A, Lahav G, Mitchison TJ (2012) Prolonged mitotic arrest triggers partial activation of apoptosis, resulting in DNA damage and p53 induction. Mol Biol Cell 23:567–576
36. Chrzanowska-Wodnicka M, Burridge K (1996) Rho-stimulated contractility drives the formation of stress fibers and focal adhesions. J Cell Biol 133:1403–1415
37. Schwartz EL (2009) Antivascular actions of microtubule-binding drugs. Clin Cancer Res 15:2594–2601. doi:10.1158/1078-0432.CCR-08-2710
38. Carmeliet P (2005) Angiogenesis in life, disease and medicine. Nature 438:932–936. doi:10.1038/nature04478
39. Lamalice L, Le Boeuf F, Huot J (2007) Endothelial cell migration during angiogenesis. Circ Res 100:782–794. doi:10.1161/01.RES.0000259593.07661.1e
40. Boyden S (1962) The chemotactic effect of mixtures of antibody and antigen on polymorphonuclear leucocytes. J Exp Med 115:453–466
41. Kuriyama S, Yamazaki M, Mitoro A et al (1998) Analysis of intrahepatic invasion of hepatocellular carcinoma using fluorescent dye-labeled cells in mice. Anticancer Res 18:4181–4188
42. Horan PK, Melnicoff MJ, Jensen BD, Slezak SE (1990) Chapter 42 Fluorescent cell labeling for in vivo and in vitro cell tracking. Methods Cell Biol. Elsevier, 469–490
43. Hofmann UB, Houben R, Bröcker E-B, Becker JC (2005) Role of matrix metalloproteinases in melanoma cell invasion. Biochimie 87:307–314. doi:10.1016/j.biochi.2005.01.013
44. Orgaz JL, Sanz-Moreno V (2013) Emerging molecular targets in melanoma invasion and metastasis. Pigment Cell Melanoma Res 26:39–57. doi:10.1111/pcmr.12041
45. Mikaelian I, Buness A, de Vera-Mudry M-C et al (2010) Primary endothelial damage is the mechanism of cardiotoxicity of tubulin-

binding drugs. Toxicol Sci 117:144–151. doi:10.1093/toxsci/kfq189
46. Lin H-L, Chiou S-H, Wu C-W et al (2007) Combretastatin A4-induced differential cytotoxicity and reduced metastatic ability by inhibition of AKT function in human gastric cancer cells. J Pharmacol Exp Ther 323:365–373. doi:10.1124/jpet.107.124966
47. Werr J, Xie X, I-Iedqvist P et al (1998) B-integrins are critically involved in neutrophil locomotion in extravascular tissue in vivo. J Exp Med 18712091–2096
48. Huttenlocher A, Horwitz AR (2011) Integrins in cell migration. Cold Spring Harb Perspect Biol 3:a005074–a005074. doi:10.1101/cshperspect.a005074
49. Zamir E, Geiger B (2001) Molecular complexity and dynamics of cell-matrix adhesions. J Cell Sci 114:3583–3590
50. Van Nieuw Amerongen GP, van Hinsbergh VWM (2001) Cytoskeletal effects of Rho-like small guanine nucleotide-binding proteins in the vascular system. Arterioscler Thromb Vasc Biol 21: 300–311. doi:10.1161/01.ATV.21.3.300
51. Haston WS, Shields JM, Wilkinson PC (1982) Lymphocyte locomotion and attachment on two-dimensional surfaces and in three-dimensional matrices. J Cell Biol 92:747–752
52. Weis SM, Cheresh DA (2011) Tumor angiogenesis: molecular pathways and therapeutic targets. Nat Med 17:1359–1370. doi:10.1038/nm.2537
53. Pàez-Ribes M, Allen E, Hudock J et al (2009) Antiangiogenic therapy elicits malignant progression of tumors to increased local invasion and distant metastasis. Cancer Cell 15:220–231. doi:10.1016/j.ccr.2009.01.027
54. Ebos JML, Lee CR, Cruz-Munoz W et al (2009) Accelerated metastasis after short-term treatment with a potent inhibitor of tumor angiogenesis. Cancer Cell 15:232–239. doi:10.1016/j.ccr.2009.01.021